hydrogen storage in Ti-Fe-Hf alloys
compmatphys project 2025-2026

Bjorn De Busschere* and Rostislaw Ashurkov†
(Dated: December 6, 2025)

In this study we present a computational investigation of hydrogen storage in TiFe and adjacent alloys, as cheap alternatives for solid state hydrogen battery materials. Using the Quantum-Espresso DFT package, we assess the computational and physical stability of these alloy structures through convergence tests and relaxation calculations. After determining their ground-state geometries, we examine hydrogen insertion by placing hydrogen atoms in interstitial sites. These simulations help identify strategies for reducing hydrogen insertion energies across different intermetallic structures. Our results show that both TiFeH and $TiFeH_2$ have negative formation energies, indicating that these compounds can form in nature and may be promising candidates for hydrogen storage. The calculations also reveal that hydrogen atoms preferentially occupy the [Ti4Fe2] octahedral sites. These results offer a computational complement to experimental studies, improving overall research in hydrogen storage material design.

Repository: A full overview of the code and obtained results can be found at:
`https://github.com/rashurko/Compmatphys-Project-Team2-2025-2026`

I. INTRODUCTION

Hydrogen is widely regarded as a promising energy carrier for future low-carbon technologies, however, the practical utilization of hydrogen energy depends strongly on the development of safe and efficient storage materials. In recent years Ti-Fe based alloys have garnered increasing interest as cheap and effective candidate materials for such solid-state hydrogen storage systems due to their favorable thermodynamic properties. However, TiFe suffers from activation difficulties, requiring high temperatures and pressure for initial hydrogen uptake. Moreover its efficiency is also highly effected by impurities, being easily deactivated by oxidation [1, 2]. It is therefore essential to develop a detailed understanding of the intrinsic properties that govern the behavior of this system. Density Functional Theory (DFT) is a powerful tool for obtaining such insights by predicting key thermodynamic, structural, and electronic properties at the atomic scale, which can guide future experiments in this field.

In this project we will use DFT to evaluate the thermodynamic properties of hydrogen uptake in Ti-Fe based alloys. In the first part, we perform essential preliminary calculations to determine reliable numerical parameters through convergence tests and obtain ground-state crystallographic information via structural relaxations. These calculations will form the basis for the exploratory work done in section IV. In this second part, hydrogen insertion behavior is studied by placing hydrogen atoms in interstitial sites of these optimized unit cells, followed by full geometry optimizations to quantify the behavior and energy cost of hydrogen storage.

II. METHODOLOGY

All calculations were performed using the QuantumEspresso (QE) package [3–5], versions 7.3. For all materials we used PAW pseudopotentials from the Standard Solid State Pseudopotential (SSSP) library [6], which provides systematically validated potentials, optimized for efficient and accurate calculations. The pseudopotentials are based on the PBE (Perdew–Burke–Ernzerhof) exchange–correlation functional and include scalar-relativistic corrections and non-linear core corrections. For the considered transition metals (Ti, Fe, Hf, Ni), the valence shells include the relevant s, p, and d states to ensure an accurate description of metallic bonding.

III. NUMERICAL EXPLORATION OF METALLIC ALLOY DFT-CALCULATIONS

A. Convergence testing

As is common in DFT, optimal computational parameters first have to be determined through a convergence test, to ensure robust and accurate calculations. Since all crystal structures considered in this paper have a similar chemical buildup, we will use the body-centered cubic TiFe crystal (see Fig. 1) as a reference material and use the found parameter values for this crystal for all calculations in this paper. As a common procedure, the parameters will be tuned with respect to the convergence of the hydrostatic pressure. First, the density of the k-mesh is incrementally increased until pressure converged within a few kbar. Similarly, we subsequently tune the values for plane-wave cutoff energy *ecutwfc* and the charge density cutoff energy *ecutrho* until reasonable final convergence is achieved. This procedure results in a standard set of parameters that will be used in all further calculations. The k-mesh size is set to 15x15x15, while the kinetic energy cutoff values are defined as *ecutwfc* = 124Ry and *ecutrho* = 1736Ry.

B. Geometry optimization for TiFe

To validate the parameters determined in the previous subsection III A, the $E(V)$ curve of the TiFe crystal was constructed. For this purpose, the *vc-relax* optimization method was used. This allows the calculation of the total energy E, cell volume V and optimal atomic positions of the unit cell for a given target pressure P.

* University of Antwerp, Department of Physics: Bjorn.DeBusschere@student.uantwerpen.be
† University of Ghent, Department of Physics: rostislaw.ashurkov@ugent.be

A set of external pressures was generated, ranging from −261.95GPa to 361.95GPa in increments of $\Delta P = 41.67$GPa, resulting in a total of 12 DFT calculations. The resulting (V, E) data points were fitted using the Birch–Murnaghan equation of state (Eq. C1). The two corresponding fits are shown in Fig. 2. The blue curve represents the fit using all data points. Since the Birch–Murnaghan equation is reliable only within approximately 10% volume variation, a second fit was performed using only the red points, yielding the red curve. Both fits give essentially identical equilibrium properties: $V_0 = 173.99$a.u.^{3}, $B_0 = 192.6$GPa, $B_1 = 4.21$, $E_0 = -448.58683$Ry. Comparing these results to the values reported by the Materials Project (denoted by an asterisk): $V_0^* = 171.27$a.u.^{3}, $B_0^* = 199$GPa [7], shows good agreement. This indicates that the chosen DFT input parameters are reasonable.

A full geometry optimization (*vc-relax*) of TiFe yields an equilibrium volume of $V_0^{\mathrm{f}} = 171.2590$a.u.^{3}. This result is in excellent agreement with the Materials Project value, V_0^*. Applying an external pressure of $P = 100$kbar results in a total energy increase of only $\Delta E = 0.0027$Ry relative to the equilibrium configuration. The corresponding unit cell volume is $V_P = 166.04885$a.u.^{3}, which represents a decrease of 3.0%. Using the simple Murnaghan equation of state (Eq. C2), which is considered valid for volume changes up to 5%, a volume change of 4.5% is predicted. This prediction is of the same order of magnitude as the change obtained from the performed geometry optimization.

C. Geometry optimization for Ti-Fe, Hf-Fe, and Ti-Ni crystal phases

The geometry optimizations for the crystals, summarized in Table II, were carried out using the same *ecutwfc* and *ecutrho* values as in subsection III A. The k-point mesh was scaled relative to that for the TiFe standard set. The updated mesh components k_i' $(i = 1, 2, 3)$ were computed as $k_i' = \mathrm{ceil}\left(\frac{A_i}{A_i'} k_i\right)$, where A_i' is the largest Cartesian component of the i-th lattice vector of the new crystal, A_i is the corresponding lattice parameter of TiFe, and k_i is the TiFe standard set mesh component (here $k_i = 15\ \forall i$). All calculations were first performed using a non-magnetic *vc-relax* calculation to obtain a reliable estimate of the cell parameters. Subsequently, an *scf* calculation with magnetization enabled was carried out, using the output of the initial *vc-relax* step, to determine whether the material exhibits magnetic ordering. Finally, a magnetic *vc-relax* calculation was performed, using the magnetic moments obtained from the *scf* calculation as the initial guess.

Using the total energies $E(AB_x)$ from these geometry optimizations, we compute the formation energy as $E_{\mathrm{form}} = E(AB_x) - E(A) - xE(B)$. From these formation energies, the phase diagrams shown in Fig. 3 are constructed. These diagrams predict that TiFe (Pm-3m), $TiFe_2$ (Fd-3m), HfFe (Pm-3m), $HfFe_2$ (Fd-3m), TiNi (Pm-3m), and $TiNi_2$ (Fd-3m) are stable and should therefore occur in nature. However, OQMD predicts a lower-energy structure for HfFe in the Pmma space group [8], while The Materials Project [7] reports TiNi (Pm-3m) and $TiNi_2$ (Fd-3m) as unstable. Based on our results, we therefore predict that TiFe (Pm-3m), $TiFe_2$ (Fd-3m), and $HfFe_2$ (Fd-3m) should appear in nature.

Our predictions are consistent with the fact that these compounds are experimentally observed [7].

IV. NUMERICAL SIMULATION OF HYDROGEN STORAGE IN INERMETALLIC ALLOYS.

A. Single hydrogen insertion in TiFe interstitial positions

To gain a general understanding of the numerical and physical implications of placing hydrogen atoms at interstitial positions, we first explore single hydrogen insertion in the cubic TiFe crystal phase. First, we look at the computational properties of this system. We do this by placing a single hydrogen atom at an unoccupied, high symmetry position and *(1) test whether physically equivalent structures are also computationally equivalent*, and *(2) see if our convergence parameter values are still valid*. TiFe exhibits a cubic Pm-3m symmetry group for which the highest symmetry Wyckoff positions, 1a and 1b, are occupied by respectively Ti and Fe. The unoccupied positions with the highest symmetry are the 3c and 3d positions (center of faces and edges). We first formulate an answer to the first question by testing whether the arbitrary choice between placing the H-atom in the symmetrically equivalent positions $(1/2, 1/2, 0)$, $(0, 1/2, 1/2)$ or $(1/2, 0, 1/2)$ leads to the same computational results. Performing a *vc-relax* calculation for these three configurations with the same conditions resulted in three times a total energy of -449.753Ry and a volume increase of 9.99%. As expected symmetrically equivalent configurations lead to equivalent computational results. Next, we answer the second question by relaxing the structure with a hydrogen atom placed in the $(0, 1/2, 1/2)$ position, now with increasing convergence parameters. The results (table I) show that increasing the convergence parameters values only leads to a minimal change in the energy of the order of 1.5×10^{-4}Ry, which is much smaller than the energy difference comparisons we will make in the rest of this paper. The difference in volume is a little bigger, but still only on the order of 0.04%. However, because the total energy shows negligible variation, the initial convergence parameters provide adequate accuracy while maintaining computational efficiency.

TABLE I: Convergence behavior of the TiFe alloy. If not specified the standard set convergence parameters from section III A are used.

Parameters	V (a.u.^{3})	ΔV (a.u.^{3})	E (Ry)	ΔE (Ry)
$k = 15$ *(original)*	191.347	—	-449.7533	—
$k = 18$	191.382	0.035	-449.7532	1.18×10^{-4}
$k = 21$	191.384	0.0024	-449.7532	1.45×10^{-4}
k=21, wfc=150, ρ=2000	191.462	0.078	-449.7534	-6.6×10^{-5}

Knowing the numerical behavior of this system, we can move on to finding the interstitial position(s) that the H-atom will occupy when inserted into the unit cell. In this section, we will always assume the insertion of one hydrogen atom per unit cell. To find the optimal positions, we perform a series of relaxation calculations, where we place the hydrogen atom at different Wyckoff positions of the original Pm-3m space group,

with increasingly lower symmetry. After these calculations are finished we take note of the final position of the hydrogen atom and the insertion energy per H-atom (in this case just 1). This insertion energy is calculated by comparing the resulting total energy with ground state energies for TiFe and atomic hydrogen, using Eq. C3. All tested positions and results from these calculations are shown in table III. Based on these results, we can confidently conclude that the $(0, 1/2, 1/2)$ position is the most energetically favorable, with an insertion energy of $E_{ins}/H = -0.1666$Ry. In this position the H-atom sits in the center of the face in the [Ti4Fe2] octahedral site. Other initial H positions yield the same insertion energy, but an inspection of the relaxed coordinates shows that the H-atom consistently migrates toward the center of the corresponding face during relaxation. This indicates that, although the insertion energies are identical, the underlying potential-energy landscape in this region is probably relatively flat. Consequently, several nearby interstitial sites are energetically equivalent, and symmetry considerations suggest that the true equilibrium position is the high-symmetry face-centered site to which the H-atom relaxes.

Clearly, these results suggest that the hydrogen atom prefers to sit on the face of the unit cell and more specifically in the center. Therefore, complementary to these results, we investigate the energy landscape of the unit cell for hydrogen positions on the face. More specifically, we expanded the original TiFe unit cell orthorhombicly by 10% in accordance with the expansions of previous relaxation calculations and performed static (*scf*) energy calculations with the H-atom placed on a 25×25 grid of points across one face of the unit cell. The resulting energy landscape is shown in Fig. 4. This plot clearly supports the fact that the [Ti4Fe2] octahedral site is the most energetically favorable, while also showcasing the subtle flatness of the energy landscape around this position. In addition, this plot also explains the seemingly stable [Ti2Fe4] octahedral site in the center of the edges. Even though the H-atom does not sit in the most energetically favorable positions, it does inhibit a completely symmetric energy potential saddle point, leading to it remaining in place during relaxation.

We find that the insertion of one hydrogen atom per formula unit into the [Ti4Fe2] octahedral sites of TiFe appears highly exothermic, with an atomic insertion energy of $E_{ins}/H = -0.1666\text{Ry} \approx -2.26\text{eV}$. In practical hydrogen storage applications, however, hydrogen is always supplied as H_2, so the relevant thermodynamic quantity is the formation energy with respect to $\frac{1}{2}H_2$, which corresponds to the hydride-formation reaction:

$$\mathrm{M} + \frac{x}{2}\mathrm{H_2} \rightarrow \mathrm{MH}_x \tag{1}$$

Where $x = 1$ for our case. The formula for calculating this formation energy and a conversion from the atomic-H insertion energy is given in the appendix. Using Eq. C8 we find a formation energy of $E_{form} = -2.26\text{eV} + 2.2693\text{eV} \approx +0.00236\text{eV/H}$ corresponding to $\approx +0.228$kJ/mol H or $+0.445$kJ/mol H_2. These results suggest that the formation of TiFeH from TiFe and gaseous H_2 is marginally endothermic. In pure electronic terms, this result suggests that the TiFeH phase is slightly unstable with respect to decomposition into the elemental components at 0K. In literature it is also reported that H will occupy the octahedral [Ti4Fe2] sites, which is consistent with what we found, however, they report formation energies in the range of -21 to -29kJ/mol H_2 [9], far below what we found. These published values include vibrational zero-point energy (ZPE) corrections, which we have not considered up until now. ZPE corrections for interstitial H in metals are non-negligible, for TiFeH being of the order of $+10$kJ/mol H_2 [9–11], and therefore strongly affect the sign and magnitude of the final formation energy. The ZPE-corrected formation energy is given in C9. This makes it hard to compare results directly. Nevertheless, if we were to apply this correction as reported in literature to our found value for the formation energy, we would move even further away from the expected energy range.

To check consistency with literature we relaxed the reportedly ground-state orthorhombic FeTiH ($P222_1$) structure [2], shown in Fig. 5. Using this crystal structure we obtain a formation energy of $E_{form} = -20.89$kJ/mol H_2, which after the same corrections cited in the literature becomes ≈ -11kJ/mol H_2. While still not fully agreeing with the expected energy range from literature, the magnitude and sign of this result is comparable and variations can most likely be attributed to the high sensitivity of the ZPE/H contributions to small structural/DFT details. A full calculation of the ZPE corrections would take us beyond the scope of this project and was not performed. The reason we don't find this structure using our previous relaxation calculations, is because the orthorhombic TiFeH phase cannot be obtained by relaxing a single TiFe unit cell with one H-atom. Although the H-atom still occupies (some of) the [Ti4Fe2] octahedral sites, which site is occupied changes between neighboring TiFe cells. Additionally, the surrounding lattice in the orthorhombic cell shows distortion across multiple neighboring TiFe cells. These symmetry-lowering distortions can only appear in relaxation calculations using larger supercells, explaining why our single-cell calculation does not reproduce the full hydride structure or its corresponding formation energy. Upon inspection of the orthorhombic FeTiH structure from literature (Fig. 8, top panel), it can be seen that one would need a supercell containing four TiFe unit cells ($2 \times 2 \times 1$) with four H-atoms occupying specific [Ti4Fe2] octahedral sites as shown in the middle panel. Theoretically, one could place these H-atoms in the same octahedral site in each TiFe cell and find this configuration through relaxation, however, the *vc-relax* operation only finds the optimal configuration *in the neighborhood* of the original configuration. This means that large 'jumps', like the H-atom moving from one face to another, are not possible. The results of the relaxation calculation with the defined supercell is shown in the bottom panel. Structurally, the relaxed configuration shows great agreement with the configuration from literature. Shown in purple is the length of the a-unit vectors in both lattices, which differ only by 0.012Å. For the relaxed structure, we calculate a formation energy of -0.00799eV, corresponding to -20.98kJ/mol H_2. This is in excellent agreement with the relaxation calculation of the orthorhombic TiFeH structure from literature, for which we found a formation energy of $-0.00796\text{eV} \approx -20.89$kJ/mol H_2 (before ZPE corrections).

In summary, we successfully identified the optimal H position and reproduced the ground-state TiFeH structure, but only because prior experimental insight guided us toward the correct configuration. Had we attempted to discover this structure using DFT alone, substantially more exhaustive

testing, using multiple larger supercells, would have been required. Our results clearly demonstrate the necessity of using larger supercells in DFT relaxation calculations, as the true TiFeH structure cannot emerge from a single-cell approach. Finally, although direct comparison with literature values is hindered since we don't know the exact ZPE corrections for our structures, the internal consistency of this correction still allows for meaningful qualitative and relative comparisons within this paper.

B. Hydrogen insertion in Ti-Fe alloys

Knowing now the preferred interstitial site for hydrogen in cubic TiFe, we next search for other energetically favorable sites in related Ti–Fe alloys. Specifically, we examine interstitial positions in both $TiFe_2$ phases discussed and relaxed in section III C. These calculations are quite intensive, not only is the unit cell significantly larger, containing more atoms, but they also require magnetism. To keep the calculations manageable, we will limit ourself to only testing high symmetry Wyckoff positions as possible interstitial sites. We believe the results from the previous section make this approach justifiable. In both cases we also tested a geometrically optimal interstitial position, calculated using the web-based platform XRDlicious [12], which, among other things, finds positions in provided unit cells which maximize the total distance to neighboring atoms. The results from these calculations are found in table IV and V. Since the cubic $TiFe_2$ unit cell is much bigger, containing four formula units, one needs to insert more H-atoms into the unit cell to achieve comparable H concentration as the TiFeH phase. For the cubic $TiFe_2$ phase we went up to 32 H-atoms. This leaves three available Wyckoff positions that could be completely filled: 8b, 16c, 32e, however, the calculations show that non of these positions had a lower E_{form} compared to the TiFeH phase. Lower symmetry positions were also tested with single hydrogen insertion. These were an 48f position and a 96g position. The 48f position has one degree of freedom, which was optimized through relaxation. The 96g site has two degrees of freedom and is also geometrically favorable, as a position with this symmetry was independently identified using the XRDlicious application. By far, the lowest energy positions was the 96g position. This clearly shows that the hydrogen prefers to sit in larger interstitial holes rather than in positions with high local symmetry.

For the hexagonal unit cell on the other hand, we went up to 6 atoms per unit cell to achieve a comparable H concentration. This leaves five unoccupied Wyckoff positions that could be completely filled: 2b, 2c, 2d, 4e and 6g. Unfortunately some of these calculations were computationally quite unstable and were not able to converge. The positions for which the formation energy was able to be calculated, were also not energetically more favorable compared to the TiFeH phase. An additional geometrically optimal position found through the XRDlicious application, was also tested (pos = (0, 0, 0.309188)), but this calculation also did not converge. In conclusion, across these two $TiFe_2$ phases, there were no interstitial sites found that were more energetically favorable compared to the TiFe 3c position, moreover, no positions were found which would result in spontaneous, exoteric hydride-formation reactions. Based on literature, the $TiFe_2$ is indeed not expected to interact with hydrogen, which is consistent with our results [2].

C. $TiFeH_x$ compounds

The search for optimal hydrogen positions in $TiFeH_x$ compounds using DFT requires the use of supercells and the evaluation of multiple initial configurations, as discussed in subsection IV A. Nevertheless, performing DFT calculations using only one of the possible initial configurations can still provide valuable insight into how the formation energy evolves with hydrogen concentration in $TiFeH_x$. This approach was demonstrated by Nong et al. in [13], where the formation energies associated with hydrogen occupying the octahedral sites [Ti2Fe4] and [Ti4Fe2] were computed for varying hydrogen contents. Tested values were: $x \in \{0.125, 0.25, 0.5, 1.0, 2.0\}$.

In this subsection, we present the results of DFT calculations (without ZPE correction) on 2×2×2 $TiFeH_x$ supercells with hydrogen placed in either the [Ti2Fe4] or [Ti4Fe2] octahedral sites. A supercell for $TiFeH_{0.5}$ is shown in Fig. 9, supercells for other values of x were constructed by either removing hydrogen atoms from this structure or adding additional hydrogen atoms to it. The [Ti2Fe4] supercells were generated by swapping the Ti and Fe atoms in the input structure of a [Ti4Fe2] supercell.

The results are shown in Fig. 10. It can be seen that the [Ti2Fe4] site consistently yields a higher formation energy, indicating that hydrogen preferentially occupies the [Ti4Fe2] octahedral site, in agreement with [13]. The TiFeH compound with hydrogen in the [Ti4Fe2] site exhibits a positive formation energy, which differs from the result obtained in Subsection IV A. This discrepancy arises because the initial structure used here is not close to the optimal configuration. Nevertheless, even with these non-optimal initial guesses, the formation energy for $TiFeH_2$ with hydrogen in [Ti4Fe2] sites is negative, consistent with [14], suggesting that such a structure may be realizable in nature.

V. CONCLUSION

Using DFT calculations on a 2×2×1 TiFeH supercell, together with prior experimental insight, we identified the optimal hydrogen position in the ground-state TiFeH structure. The corresponding formation energy, -20.98 kJ/mol H_2, shows excellent agreement with values reported in the literature; however, it should be noted that no ZPE correction was applied, which could significantly affect the result. Furthermore, the results demonstrate that hydrogen atoms preferentially occupy the [Ti4Fe2] octahedral sites rather than the [Ti2Fe4] sites, and that $TiFeH_2$ exhibits a negative formation energy, indicating that this phase may be relevant for hydrogen storage applications. However, the optimal structure of $TiFeH_2$ could not be conclusively determined in this work, meaning that its formation energy is not yet known with sufficient accuracy to be directly compared to that of TiFeH. Therefore, additional investigation of the $TiFeH_2$ compound is required to determine whether it is less stable than TiFeH, which would make it the more reversible hydride and potentially a better candidate for hydrogen storage.

[1] P. Modi and F. Aguey-Zinsou, Frontiers in Energy Research **9**, 616115 (2021).

[2] H. Liu, Z. Jingxi, P. Sun, C. Zhou, Y. Liu, and Z. Fang, Journal of Energy Storage **68**, 107772 (2023).

[3] P. Giannozzi, O. Andreussi, T. Brumme, O. Bunau, M. B. Nardelli, M. Calandra, R. Car, C. Cavazzoni, D. Ceresoli, M. Cococcioni, N. Colonna, I. Carnimeo, A. D. Corso, S. de Gironcoli, P. Delugas, R. A. D. Jr, A. Ferretti, A. Floris, G. Fratesi, G. Fugallo, R. Gebauer, U. Gerstmann, F. Giustino, T. Gorni, J. Jia, M. Kawamura, H.-Y. Ko, A. Kokalj, E. Küçükbenli, M. Lazzeri, M. Marsili, N. Marzari, F. Mauri, N. L. Nguyen, H.-V. Nguyen, A. O. de-la Roza, L. Paulatto, S. Poncé, D. Rocca, R. Sabatini, B. Santra, M. Schlipf, A. P. Seitsonen, A. Smogunov, I. Timrov, T. Thonhauser, P. Umari, N. Vast, X. Wu, and S. Baroni, Journal of Physics: Condensed Matter **29**, 465901 (2017).

[4] P. Giannozzi, S. Baroni, N. Bonini, M. Calandra, R. Car, C. Cavazzoni, D. Ceresoli, G. L. Chiarotti, M. Cococcioni, I. Dabo, A. Dal Corso, S. de Gironcoli, S. Fabris, G. Fratesi, R. Gebauer, U. Gerstmann, C. Gougoussis, A. Kokalj, M. Lazzeri, L. Martin-Samos, N. Marzari, F. Mauri, R. Mazzarello, S. Paolini, A. Pasquarello, L. Paulatto, C. Sbraccia, S. Scandolo, G. Sclauzero, A. P. Seitsonen, A. Smogunov, P. Umari, and R. M. Wentzcovitch, Journal of Physics: Condensed Matter **21**, 395502 (19pp) (2009).

[5] P. Giannozzi, O. Baseggio, P. Bonfà, D. Brunato, R. Car, I. Carnimeo, C. Cavazzoni, S. de Gironcoli, P. Delugas, F. Ferrari Ruffino, A. Ferretti, N. Marzari, I. Timrov, A. Urru, and S. Baroni, The Journal of Chemical Physics **152**, 154105 (2020), https://doi.org/10.1063/5.0005082.

[6] G. Prandini, A. Marrazzo, I. E. Castelli, N. Mounet, and N. Marzari, npj Computational Materials **4**, 72 (2018), http://materialscloud.org/sssp.

[7] M. de Jong, W. Chen, T. Angsten, A. Jain, R. Notestine, A. Gamst, M. Sluiter, C. Krishna Ande, S. van der Zwaag, J. J. Plata, C. Toher, S. Curtarolo, G. Ceder, K. A. Persson, and M. Asta, Scientific Data **2**, 150009 (2015).

[8] J. E. Saal, S. Kirklin, M. Aykol, B. Meredig, and C. Wolverton, JOM (1989) **65**, 1501 (2013).

[9] S. P. Padhee, A. Roy, and S. Pati, International Journal of Hydrogen Energy **46**, 906.

[10] ResearchGate 10.1103/PhysRevB.76.064207.

[11] C. Wolverton, Physical Review B **69**, 10.1103/PhysRevB.69.144109.

[12] M. Lebeda *et al.*, Applied Crystallography **58** (2025).

[13] Z.-S. Nong, J.-C. Zhu, X.-W. Yang, Y. Cao, Z.-H. Lai, and Y. Liu, Computational Materials Science **81**, 517 (2014).

[14] L. Mohammedi, B. Daoudi, and A. Boukraa, Computational Condensed Matter **2**, 11 (2015).

[15] N. C. WebBook, Hydrogen (h_2) — diatomic spectroscopic constants, `https://webbook.nist.gov`, see Huber & Herzberg (1979).

Appendices

Appendix A: Figures

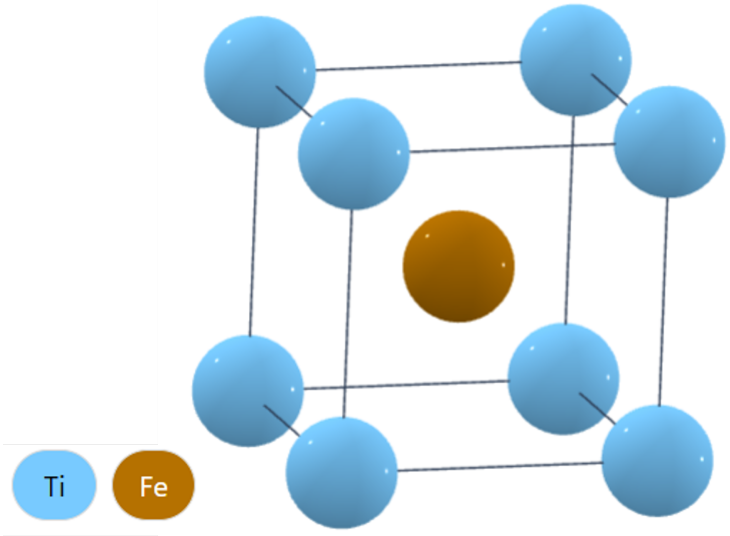

FIG. 1: TiFe in the cubic Pm-3m crystal structure.

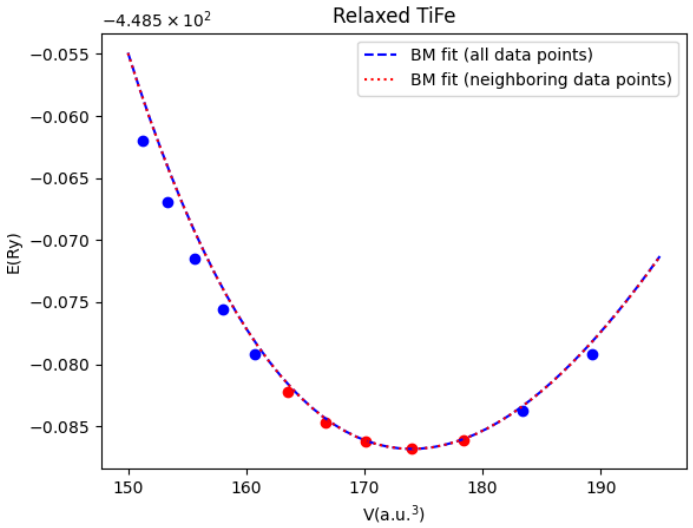

FIG. 2: The $E(V)$ curve of the TiFe unit cell in the cubic Pm-3m crystal structure. Shown are the Birch–Murnaghan fit using all data points (blue & red) and the fit restricted to the neighboring points near the minimum (red).

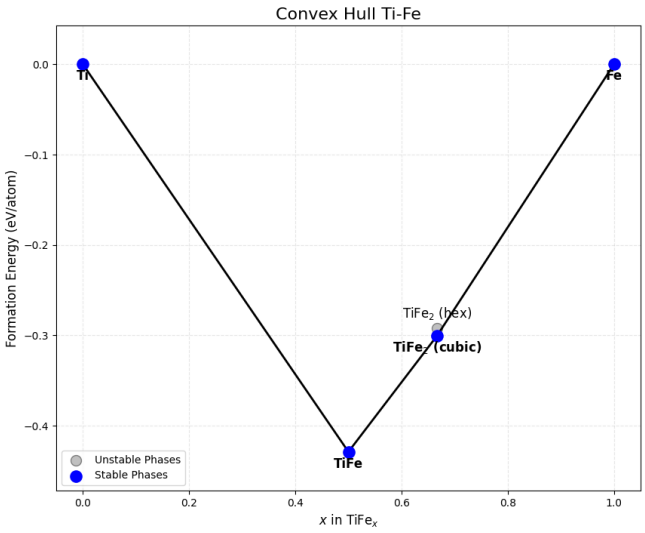

(a) Ti-Fe phase diagram.

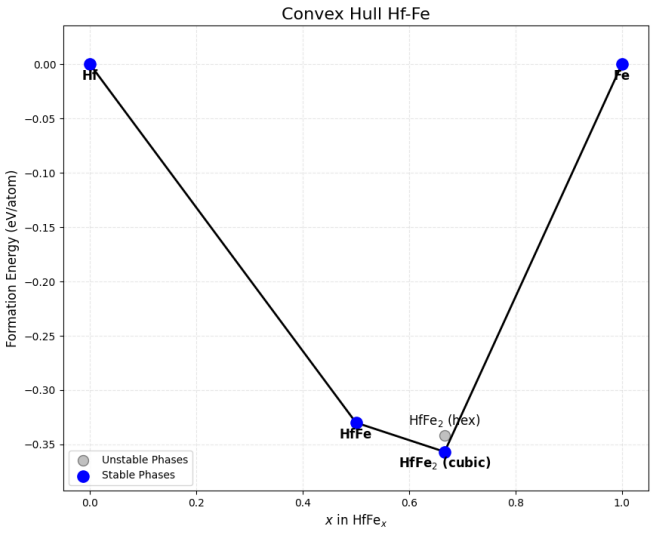

(b) Hf-Fe phase diagram.

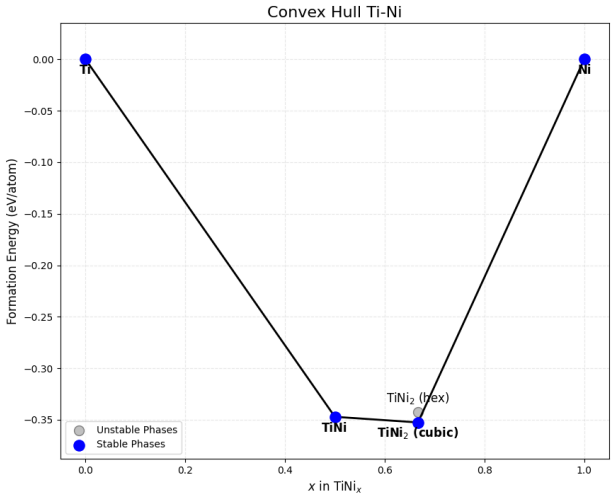

(c) Ti-Ni phase diagram.

FIG. 3: Calculated convex hull phase diagrams for the Ti-Fe, Hf-Fe, and Ti-Ni binary systems. The calculated formation energy values are listed in table II.

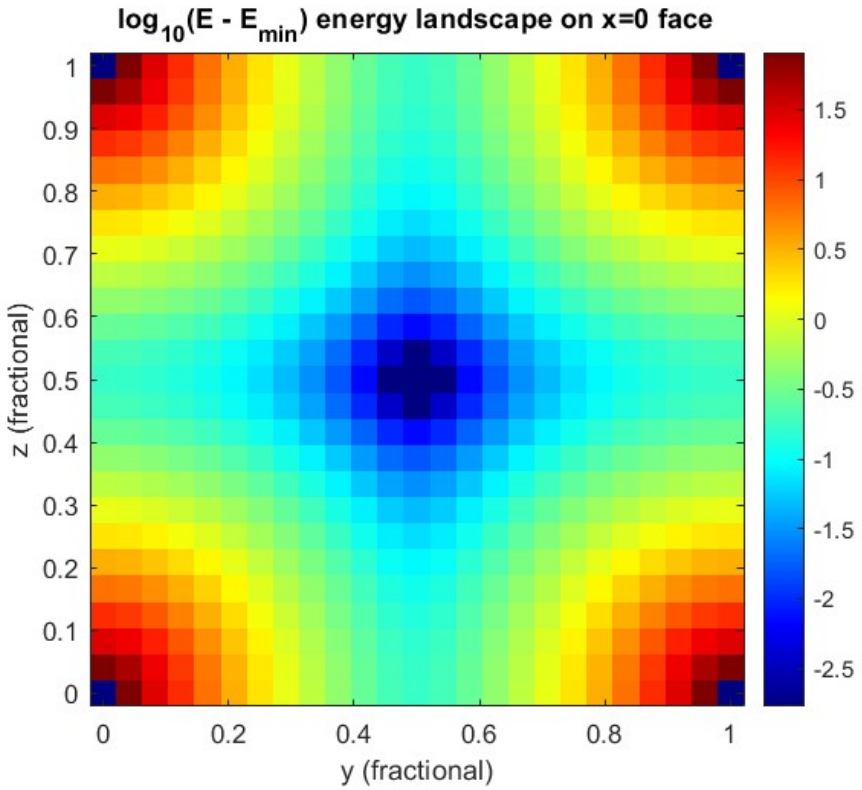

FIG. 4: Energy landscape on the x=0 face of TiFe, showing $\log_{10}(E - E_{min})$ for a hydrogen atom sampled over a 25×25 grid.

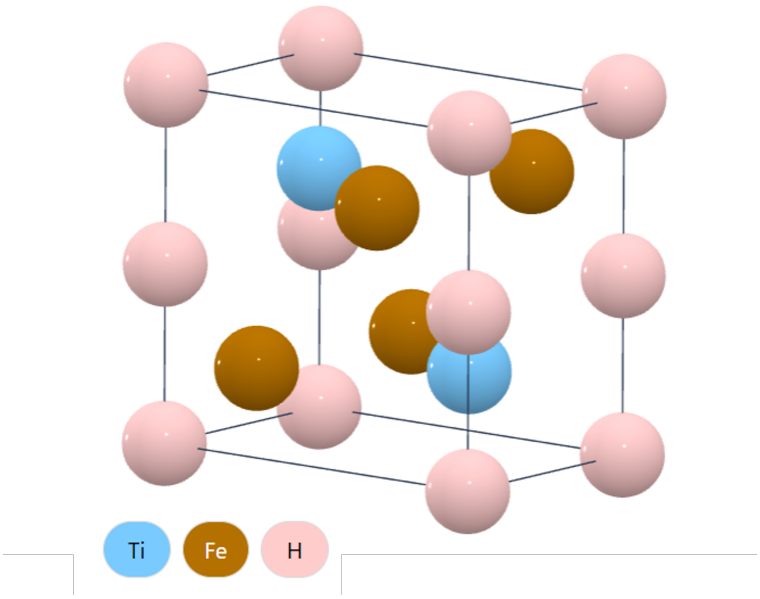

FIG. 5: TiFeH in the orthorhombic $P222_1$ crystal structure.

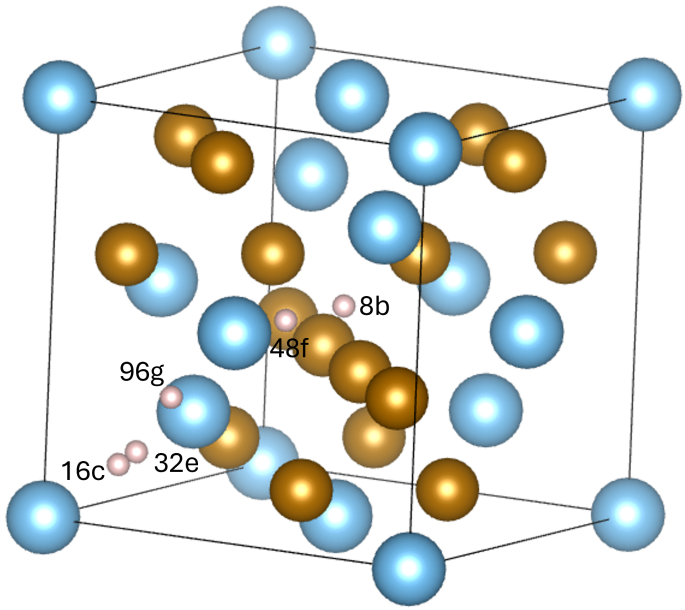

FIG. 6: Visualization of the different interstitial Wickoff positions tested for hydrogen insertion formation energy in the cubic $TiFe_2$ phase. The exact coordinates evaluated are: 8b: (0.5,0.5,0.5), 16c: (0.125,0.125,0.125), 32e: (0.155,0.155,0.155), 48f: (0.5,0.5,0.235), 96f: (0.323,0.323,0.021).

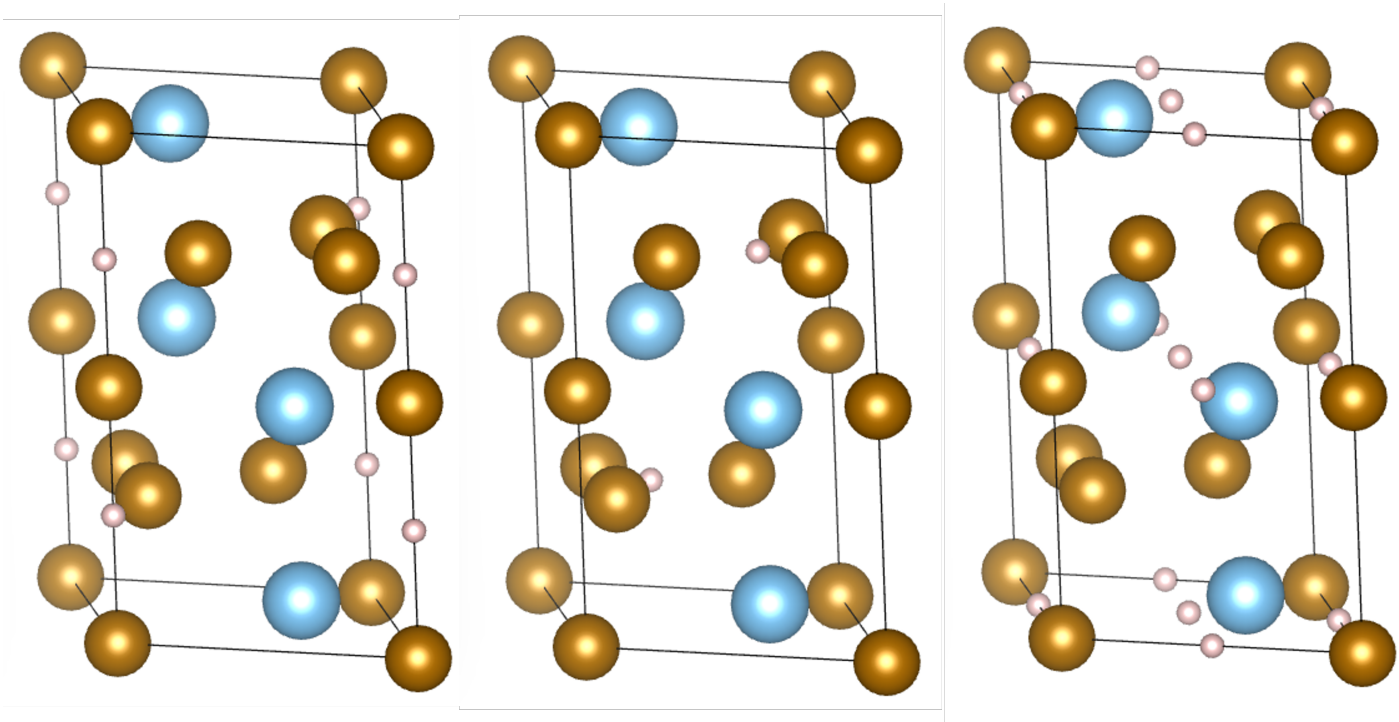

FIG. 7: Visualization of the different interstitial Wickoff positions tested for hydrogen insertion formation energy in the hexagonal $TiFe_2$ phase that were able to converge. **Left:** 2b, **Middle:** 2d, **Right:** 6g.

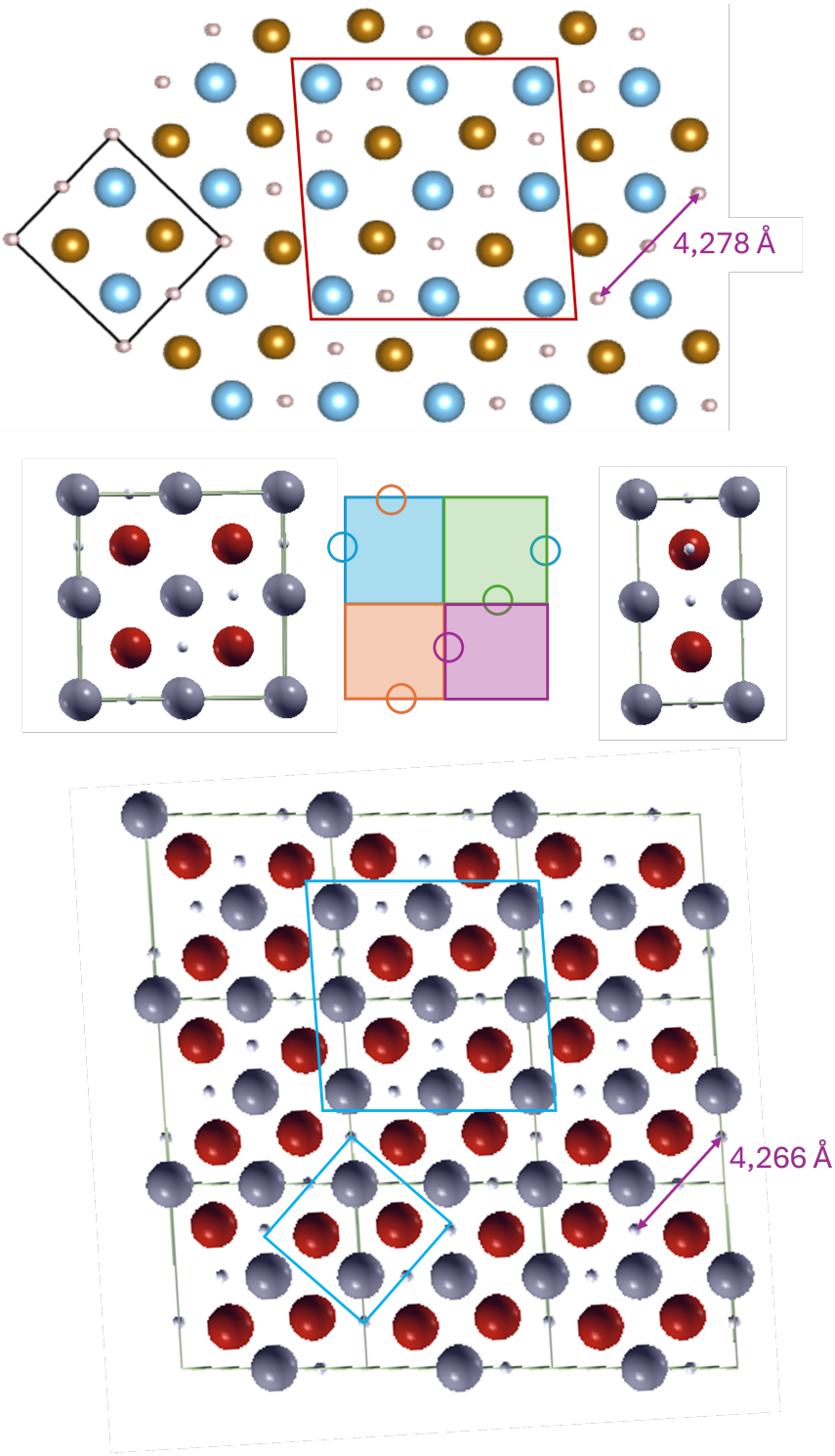

FIG. 8: **Top:** Relaxed ground-state structure of orthorhombic TiFeH phase with space group $P222_1$. The black outline marks the conventional unit cell, while the red region indicates the smallest H-filled cubic TiFe building block from which the full structure can be constructed by tiling. In these cubic TiFe fragments, all H-atoms occupy [Ti4Fe2] octahedral interstitial sites, but on different faces of adjacent unit cells. **Middle:** Cubic TiFe supercell prior to relaxation, containing four hydrogen atoms placed in [Ti4Fe2] octahedral sites at positions equivalent to those found in the orthorhombic TiFeH structure. The central image highlights the four TiFe unit cells and the corresponding H-site locations (circles), while the right image provides a side view of the same supercell. **Bottom:** Relaxed configuration of the same hydrogen-containing cubic TiFe supercell shown in the middle panel. The blue regions indicate the same structural subsections highlighted in the top figure, allowing direct comparison between the orthorhombic TiFeH structure and the relaxed hydrogen-filled cubic TiFe supercell.

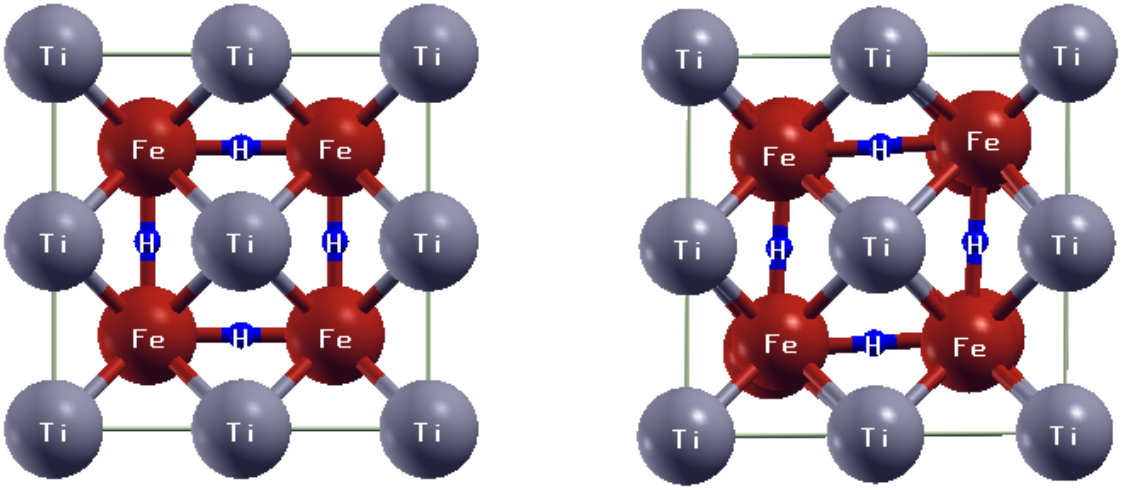

FIG. 9: $TiFeH_{0.5}$ 2×2×2 supercells, with hydrogen atoms occupying [Ti4Fe2] octahedral sites. **Left:** initial configuration, with hydrogen atoms at $(\frac{1}{2}, \frac{1}{4}, \frac{3}{4})$, $(\frac{3}{4}, \frac{1}{4}, \frac{1}{2})$, $(\frac{1}{2}, \frac{3}{4}, \frac{1}{4})$, and $(\frac{1}{4}, \frac{3}{4}, \frac{1}{2})$. **Right:** relaxed configuration after a *vc-relax* calculation.

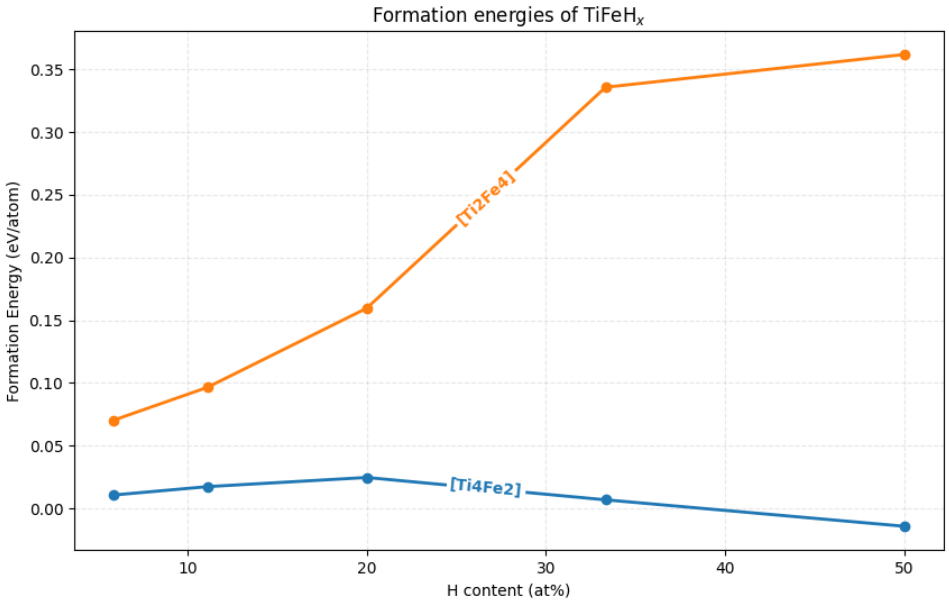

FIG. 10: Formation energies of hydrogen occupying the octahedral sites [Ti2Fe4] and [Ti4Fe2] for varying hydrogen concentrations. All energies were obtained from *vc-relax* calculations performed on 2×2×2 supercells using an 8×8×8 k-point mesh. at% describes the relative fraction of atoms in a compound. For example, when $x = 1$ in $TiFeH_x$, the hydrogen content is $\frac{1}{3}$, corresponding to 33.3 at%.

Appendix B: Tables

Material	k-mesh	Space group	E_{form} (eV/atom)
Ti	21x21x21	P6/mmm	—
Hf	21x21x21	$P6_3/mmc$	—
Ni	15x15x15	Fm-3m	—
Fe	15x15x15	Im-3m	—
TiFe	15x15x15	Pm-3m	-0.428876121
$TiFe_2$ (hexagonal)	15x15x15	$P6_3/mmc$	-0.291750417
$TiFe_2$ (cubic)	5x5x5	Fd-3m	-0.300563875
HfFe	15x15x15	Pm-3m	-0.329947403
$HfFe_2$ (hexagonal)	7x7x4	$P6_3/mmc$	-0.341658932
$HfFe_2$ (cubic)	5x5x5	Fd-3m	-0.356804796
TiNi	15x15x15	Pm-3m	-0.347125245
$TiNi_2$ (hexagonal)	9x9x9	$P6_3/mmc$	-0.34257415
$TiNi_2$ (cubic)	7x7x7	Fd-3m	-0.352589513

TABLE II: Summary of the geometry optimization results for Ti–Fe, Hf–Fe, and Ti–Ni crystals. The table lists the k-mesh values, space groups, and formation energies of the corresponding structures.

Material	Initial H position	Final H position	V (a.u.^{3})	ΔV (%)	E_{tot} (Ry)	E_{ins}/H (Ry)	H-conc (#H/a.u.^{3})
TiFe	—	—	173.9675	—	-448.5868691	—	—
H	—	—	—	—	-0.99984467	—	—
TiFeH (3c)	($\frac{1}{2}$,$\frac{1}{2}$,0)	($\frac{1}{2}$,$\frac{1}{2}$,0)	191.34049	9.9863	-449.7533307	-0.16661688	0.005226285
TiFeH (3d)	($\frac{1}{2}$,0,0)	($\frac{1}{2}$,0,0)	188.93904	8.6059	-449.7168550	-0.13014115	0.005292712
TiFeH (8g)	($\frac{1}{4}$,$\frac{1}{4}$,$\frac{1}{4}$)	(0.29630, 0.21085, 0.27394)	193.20731	11.0594	-449.7049211	-0.11820726	0.005175788
TiFeH (6f)	($\frac{1}{2}$,$\frac{1}{2}$,$\frac{1}{4}$)	(0.50000, 0.50000, 0.08334)	191.34566	9.9893	-449.7533307	-0.16661693	0.005226144
TiFeH (12j)	($\frac{1}{2}$,$\frac{1}{4}$,$\frac{1}{4}$)	(0.50000, 0.15789, 0.15789)	191.58015	10.1241	-449.7244994	-0.13778554	0.005219747
TiFeH (24l)	($\frac{1}{2}$,0.12,0.24)	(0.50000, 0.03999, 0.41338)	191.34780	9.9905	-449.7533307	-0.1666169	0.005226086
TiFeH (24m)	(0.12,0.12,0.24)	(0.11454, 0.11454, 0.41338)	191.58214	10.1252	-449.7244988	-0.13778501	0.005219693
TiFeH (48n)	(0.12,0.24,0.36)	(0.04001, 0.41335, 0.45330)	191.33847	9.9852	-449.7533306	-0.16661679	0.005226341

TABLE III: Summary of hydrogen insertion results for TiFe. Listed are the initial and final hydrogen positions, relaxed cell volumes, percent volume change relative to TiFe, total energies, insertion energies relative to TiFe + H, and hydrogen concentration.

Material	V (a.u.^{3})	ΔV (%)	E_{tot} (Ry)	E_{ins}/H (Ry)	E_{form} (Ry)	E_{form} (kJ/mol H_2)	H-conc (#H/a.u.^{3})
$TiFe_2$ (8a Ti, 16d Fe)	2080.44575	—	-6222.898788	—	—	—	—
H	—	—	-0.99984467	—	—	—	—
H_2	—	—	-2.33326984	—	—	—	—
$TiFe_2H_{0.125}$ (8b)	2117.37263	1.77495	-6224.008719	-0.11008672	0.05670353	148.8747039	0.000472283
$TiFe_2H_{0.125}$ (16c)	2105.21313	1.19048	-6223.998923	-0.10029086	0.06649939	174.5936627	0.000475011
$TiFe_2H_{0.125}$ (32e)	2105.00284	1.18038	-6224.005086	-0.10645422	0.06033603	158.4118061	0.000475059
$TiFe_2H_{0.125}$ (48f)	2101.35480	1.00503	-6224.041857	-0.14322508	0.02356517	61.87018172	0.000475883
$TiFe_2H_{0.125}$ (96g*)	2099.10140	0.89671	-6224.054655	-0.15602309	0.01076716	28.26909994	0.000476394
$TiFe_2H$ (8b)	2374.76522	14.14694	-6231.698515	-0.10012126	0.06666899	175.0389496	0.003368754
$TiFe_2H_2$ (16c)	2634.61958	26.63726	-6240.309443	-0.08832128	0.07846897	206.0196994	0.006072983
$TiFe_2H_2$ (32e: *1/2-filled*)	2634.81497	26.64666	-6240.309445	-0.08832144	0.07846881	206.0192859	0.006072533
$TiFe_2H_3$ (32e)	4803.41255	130.88382	-6253.709124	0.03702166	0.20381191	535.1066869	0.00666193

TABLE IV: Summary of hydrogen insertion results for cubic $TiFe_2$. Shown are the relaxed cell volumes, percent volume change relative to $TiFe_2$, total energies, hydrogen insertion energies (relative to $TiFe_2$ + H), and calculated formation energies relative to H_2, and hydrogen concentrations. *Note that the 96g position was found using the XRDelicious application, which provided the optimal value for the two free parameters which define this position: (x,x,z).

Material	V (a.u.^{3})	ΔV (%)	E_{tot} (Ry)	E_{ins}/H (Ry)	E_{form} (Ry)	E_{form} (kJ/mol H_2)	H-conc (#H/a.u.^{3})
$TiFe_2$ (4f Ti, 2a/6h Fe)	1034.16391	—	-3111.441763	—	—	—	—
H	—	—	-0.99984467	—	—	—	—
H_2	—	—	-2.33326984	—	—	—	—
$TiFe_2H_{0.5}$ (2b)	1058.96494	2.39817	-3113.627427	-0.09298741	0.07380284	193.7688043	0.00188864
$TiFe_2H_{0.5}$ (2c)				*did not converge*			
$TiFe_2H_{0.5}$ (2d)	1078.59827	4.29665	-3113.600067	-0.07930736	0.08748290	229.6857019	0.00185426
$TiFe_2H$ (4e)				*did not converge*			
$TiFe_2H_{1.5}$ (6g)	1215.53883	17.53831	-3118.004220	-0.09389817	0.07289208	191.3776193	0.00493608

TABLE V: Summary of hydrogen insertion results for hexagonal $TiFe_2$. Shown are relaxed cell volumes, percent volume change relative to $TiFe_2$, total energies, hydrogen insertion energies (relative to $TiFe_2$ + H), formation energies relative to H_2, and hydrogen concentrations.

Appendix C: Used Formulas

Birch-Murnaghan equations of state

$$E(V) = E_0 = \frac{9V_0B_0}{16}\left[\left(\left(\frac{V_0}{V}\right)^{\frac{2}{3}} - 1\right)^3 B_1 + \left(\left(\frac{V_0}{V}\right)^{\frac{2}{3}} - 1\right)^2 \left(6 - 4\left(\frac{V_0}{V}\right)^{\frac{2}{3}}\right)\right] \tag{C1}$$

Murnaghan volume equation

$$V(P) = V_0\left[1 + P\left(\frac{B_1}{B_0}\right)\right]^{-\frac{1}{B_1}} \tag{C2}$$

Insertion energy per atomic hydrogen

$$E_{ins}/H = [E(\mathrm{TiFe} + \mathrm{H}) - E(\mathrm{TiFe}) - \#H \times E(\mathrm{H})]/\#H \tag{C3}$$

Hydride formation energy

In our calculations we reported hydrogen insertion energies with respect to an isolated hydrogen atom. In real applications, however, hydrogen is supplied as molecular H_2, so it is useful to convert the atomic-H insertion energy into the corresponding $\frac{1}{2}H_2$-referenced quantity. This so called hydride formation energy E_{form} is defined as:

$$E_{\mathrm{form}} = E(\mathrm{TiFe} + \mathrm{H}) - E(\mathrm{TiFe}) - \tfrac{1}{2}E(\mathrm{H_2}) \tag{C4}$$

The atomic-H insertion energy we used before is:

$$E_{\mathrm{ins}}(\mathrm{H}) = E(\mathrm{TiFe} + \mathrm{H}) - E(\mathrm{TiFe}) - E(\mathrm{H}) \tag{C5}$$

Subtracting these expressions gives the relationship:

$$E_{\mathrm{form}} = E_{\mathrm{ins}}(\mathrm{H}) + \left[E(\mathrm{H}) - \tfrac{1}{2}E(\mathrm{H_2})\right] \tag{C6}$$

The bracketed term is half the H_2 bond dissociation energy,

$$E(\mathrm{H}) - \tfrac{1}{2}E(\mathrm{H_2}) = \tfrac{1}{2}D_e(\mathrm{H_2}) \tag{C7}$$

We can find the value for this dissociation energy in a consistent way by calculating the energy term $E(H_2)$ explicitly. This is done by calculating the total energy for an H_2 molecule in an otherwise empty and enlarged unit cell. This resulted in a total energy of $E(H_2) = -2.333$ Ry ≈ -31.75eV. Using this value, we can calculate the H_2 bond dissociation energy to be $D_e \approx 4.539$eV, which is in good agreement with the value found in literature $D_e \approx 4.52\,\mathrm{eV}$ [15]. Using this we can find the hydride formation energy out or the hydrogen insertion energy via:

$$E_{\mathrm{form}} = E_{\mathrm{ins}}(\mathrm{H}) + 2.2693\mathrm{eV} \tag{C8}$$

Zero point energy correction for TiFeH

$$E_{form}^{ZPE} = E_{form}^{\mathrm{DFT}} + \mathrm{ZPE[TiFeH]} - \mathrm{ZPE[TiFe]} - \frac{1}{2}\,\mathrm{ZPE[H_2]} \tag{C9}$$

in which $ZPE = \frac{1}{2}\sum_i h\nu_i$ represents the sum over the different vibrational modes.